PHYSICAL REVIEW B **88**, 140502(R) (2013)

Unusual nature of fully gapped superconductivity in In-doped SnTe

Mario Novak,[*] Satoshi Sasaki, Markus Kriener,[†] Kouji Segawa, and Yoichi Ando[‡]
Institute of Scientific and Industrial Research, Osaka University, Ibaraki, Osaka 567-0047, Japan
(Received 5 September 2013; published 7 October 2013)

The superconductor $Sn_{1-x}In_xTe$ is a doped topological crystalline insulator and has become important as a candidate topological superconductor, but its superconducting phase diagram is poorly understood. By measuring about 50 samples of high-quality, vapor-grown single crystals, we found that the dependence of the superconducting transition temperature T_c on the In content x presents a qualitative change across the critical doping $x_c \simeq 3.8\%$, at which a structural phase transition takes place. Intriguingly, in the ferroelectric rhombohedral phase below the critical doping, T_c is found to be strongly *enhanced* with impurity scattering. It appears that the nature of electron pairing changes across x_c in $Sn_{1-x}In_xTe$.

DOI: 10.1103/PhysRevB.88.140502 PACS number(s): 74.25.Dw, 74.62.Dh, 03.65.Vf, 74.70.Xa

Recently, superconductors derived from topological insulators are attracting significant attention,[1–20] because they have a potential to be topological superconductors.[21–23] Topological superconductors are characterized by a nontrivial topology of the superconducting wave functions,[21–23] and they necessarily harbor gapless surface quasiparticle states that often consist of Majorana fermions,[24] an exotic kind of particle that is its own antiparticle.

In this context, the superconductor[25,26] $Sn_{1-x}In_xTe$ is of interest, because it is derived from SnTe, which is a new type of topological insulator called a topological crystalline insulator.[27–29] Intriguingly, this material (with $x \simeq 0.045$) preserves[20] the topological surface state above T_c and, furthermore, was found to present signatures of surface Andreev bound states in the point contact spectroscopy.[18] Given that the existence of surface Andreev bound states is a hallmark of unconventional superconductivity[30] and that the symmetry of the effective Hamiltonian of $Sn_{1-x}In_xTe$ implies that an unconventional superconductivity in this material is bound to be topological,[18] $Sn_{1-x}In_xTe$ has become a strong candidate for a topological superconductor.

Because of the heightened interest in $Sn_{1-x}In_xTe$, it is important to establish its phase diagram with respect to In doping. In particular, $Sn_{1-x}In_xTe$ in the low In-doping range is known to present a ferroelectric transition at low temperature, accompanied by a structural phase transition from cubic to rhombohedral,[31–34] and the signatures of surface Andreev bound states were observed[18] for $x \simeq 0.045$, which is close to this ferroelectric phase. Therefore, it is useful to clarify the details of the superconducting phase diagram in the low In-doping range that is only poorly understood.[26] Also, since the superconducting transition temperature T_c of $Sn_{1-x}In_xTe$ is unusually high[35,36] for its carrier density of $\sim 10^{21}$ cm^{-3} and it has been proposed that impurity scattering might be *enhancing* the T_c in this system,[37] it would be interesting to see how the T_c is related to disorder in $Sn_{1-x}In_xTe$.

In this Rapid Communication, we report the phase diagram of $Sn_{1-x}In_xTe$ for $x = 0.018$–0.08 based on the measurements of 51 single-crystal samples. It was found that robust, fully gapped superconductivity is established for the entire doping range studied, but the dependence of T_c on x in the ferroelectric rhombohedral phase is clearly different from that in the cubic phase where T_c vs x is confirmed to be essentially linear, as was previously reported.[26] Our data suggest that the T_c in the rhombohedral phase is primarily governed by the level of disorder, and surprisingly, T_c tends to become *higher* in more disordered samples. This tendency seems to exist also in the cubic phase, although there the T_c is primarily determined by carrier density and the change in T_c with disorder is much weaker. Hence, even though the electron pairing is expected to be driven by electron-phonon interactions in this material,[18,36,37] there is a certain unusual aspect in the pairing mechanism.

The single crystals of $Sn_{1-x}In_xTe$ were grown by a vapor-transport method. A stoichiometric ratio of high purity elements of Sn (99.99%), In (99.99%), and Te (99.999%) were melted in an evacuated quartz tube to form a homogeneous polycrystalline source, and the quartz tube was subsequently transferred to a horizontal three-zone furnace for the single crystal growth. During the crystal growth, the source material was kept in a 1.5 K/cm temperature gradient centered at 630 °C for 1 week, after which high-quality faceted single crystals larger than 1×1 mm^2 in lateral size are obtained. The rocksalt structure (space group $Fm\bar{3}m$) of the single crystals was confirmed by x-ray diffraction analysis at room temperature. The In content x in the crystals was determined by the inductively coupled plasma atomic emission spectroscopy (ICP-AES) analysis, for which the samples were dissolved into 1 M of aqueous HNO_3. The measured x values in the vapor-grown samples were always lower than those of the source materials. We could not achieve the actual x value of more than 0.08 regardless of the In content in the source material. Transport measurements were performed using six-probe techniques down to 0.3 K in magnetic fields up to ± 14 T with the current in the [100] direction. The electrical contacts were made with Au wires using Ag paint which gave a contact resistance of <1 Ω. Specific heat was measured down to 0.34 K with a relaxation-time method using a Quantum Design physical property measurement system (PPMS-9).

Let us begin by examining the role of In doping. There are two sources of hole carriers in $Sn_{1-x}In_xTe$. The parent compound SnTe is always Sn deficient and is better written as $Sn_{1-\delta}Te$, where δ is usually around $\sim 1\%$;[31] such Sn vacancies introduce holes. The second source is the In dopants. The valence of In in $Sn_{1-x}In_xTe$ is $+1$,[26] and one hole is introduced per In atom. The ICP-AES analyses allowed us to accurately

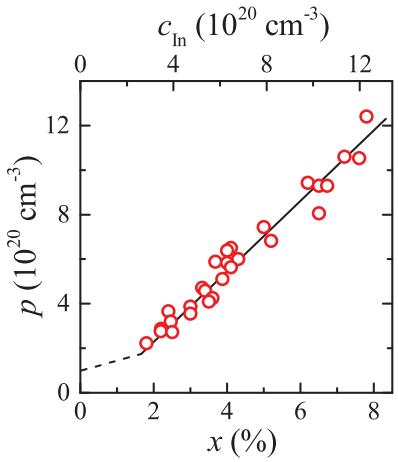

FIG. 1. (Color online) Hole density p vs x (lower axis) and c_{In} (upper axis). The solid line is a least-square fit to the data and the dashed line indicates the approximate hole density for $x = 0$–0.017 reported in Ref. 26.

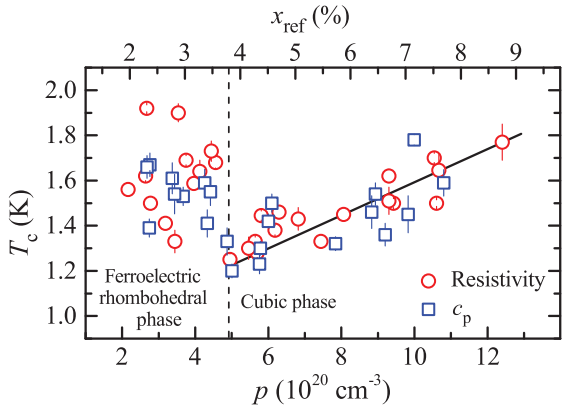

FIG. 2. (Color online) T_c vs p plot with the upper horizontal axis showing x_{ref}. Depending on the sample, T_c was measured either with resistivity (open circles) or with specific heat (open squares). The vertical dashed line marks p_c to separate the two different structure phases. The vertical error bar signifies the transition width, which was defined with the resistivity change from 90% to 10% of $\rho_{4\,K}$, or with the range between the onset and the peak in the specific-heat jump.

determine the actual In content x averaged over the whole volume of the sample, which also gives the volume density of In atoms c_{In}. Alongside this chemical analysis, we determined the hole density p from the Hall measurements in 29 samples in the following way: The Hall coefficient R_H was extracted from the slope of the Hall resistivity ρ_{yx} versus the magnetic field B, which is found to be always completely linear. Then, the nominal Hall carrier density $p_H = 1/(eR_H)$ is determined at 4 K. The true hole density can be obtained by multiplying p_H with the Hall factor r.[29] For SnTe, the Hall factor has been elucidated to be 0.6,[38] and hence one obtains p via $p = 0.6\,p_H$. As shown in Fig. 1, the relation between p and c_{In} is linear with a slope close to 1. This result reassures that the valence of In is +1 and that the Hall factor $r = 0.6$ is valid in $Sn_{1-x}In_xTe$. In a previous study,[26] it was found that for $x = 0$–0.017, p is primarily determined by Sn vacancies and saturates in the (1–2) $\times 10^{20}$ cm^{-3} range, which is also indicated in Fig. 1 with a dashed line.

Now we focus on the behavior of T_c. Figure 2 shows the T_c vs p plot for all the samples measured in this work. The T_c's of 29 samples were measured with resistivity, and those of 22 samples were measured with specific heat. In both cases, T_c is determined from the midpoint of the transition, and the error bar signifies the transition width. The data are primarily shown against p, because we found that T_c shows better systematics against p rather than against x.[39] In Fig. 2, using the upper horizontal axis, we also show x_{ref}, which is calculated from p using the linear relation found in Fig. 1, to give reference to the doping level per formula unit in this plot.

The lower limit of p where we found superconductivity is 2.2×10^{20} cm^{-3}, which corresponds to $x_{ref} \simeq 0.019$ and is consistent with the previous report.[26] However, while it was reported in Ref. 26 that T_c linearly increases with increasing x once superconductivity with $T_c > 0.3$ K is induced in samples with $x \gtrsim 0.02$, we found that such a trend only exists for p above a critical value $p_c \simeq 4.8 \times 10^{20}$ cm^{-3}, which corresponds to $x_{ref} \simeq 0.038$. Strikingly, this p_c is essentially the same as the critical hole density p_c^{FE} above which the ferroelectric rhombohedral phase disappears.[26,40] Below this critical p_c, we found that T_c shows virtually no correlation with p and spreads rather widely between 1.3 and 1.9 K. It is interesting to note that the highest T_c of 1.9 K in this study was observed in samples at low doping, $p \simeq 2.7 \times 10^{20}$ and 3.5×10^{20} cm^{-3}, and it exceeds the T_c of maximally doped samples. On the other hand, the lowest $T_c \approx 1.2$ K was only observed in samples near p_c on the cubic-structure side.

To understand this puzzling behavior, we show in Fig. 3 the plots of T_c versus the residual resistivity at 4 K, $\rho_{4\,K}$, for several p values at which three or more samples were measured. Note that $\rho_{4\,K}$ gives a measure of the strength of impurity scattering in the sample. One can see a clear trend that T_c is *enhanced* as $\rho_{4\,K}$ becomes larger. In particular, the highest T_c of 1.9 K was observed in samples with a relatively large $\rho_{4\,K}$ of 0.6–0.7 mΩ cm, which is very unusual. This unusual trend is most obvious in samples with $p < p_c$ and it is weaker for $p > p_c$, but it seems that the same trend still exists at large p. Altogether, the results shown in Figs. 2 and 3 strongly suggest that T_c is mainly determined by the unusual enhancement due to impurity scattering in the ferroelectric rhombohedral phase, while in the cubic phase it is determined primarily by p but is still affected by the impurity scattering in an unusual manner.

It is well known that in unconventional superconductors, the pairing gap is strongly suppressed by impurity scattering.[41–45] In conventional BCS superconductors, on the other hand, T_c is known to be insensitive to weak disorder.[46] The present observation is at odds with both cases, and hence is very peculiar. Nevertheless, it was argued by Martin and Phillips[37] that nonmagnetic impurities in $Sn_{1-x}In_xTe$ and $Pb_{1-x}Tl_xTe$ could enhance T_c due to their dual role of reducing the on-site Coulomb repulsion and enhancing the density of states at the Fermi energy (in this theory, the negative-U mechanism[47] is not involved). Therefore, our observation is not without theoretical justification. Apparently, more microscopic studies to elucidate the pairing mechanism in $Sn_{1-x}In_xTe$ are strongly called for.

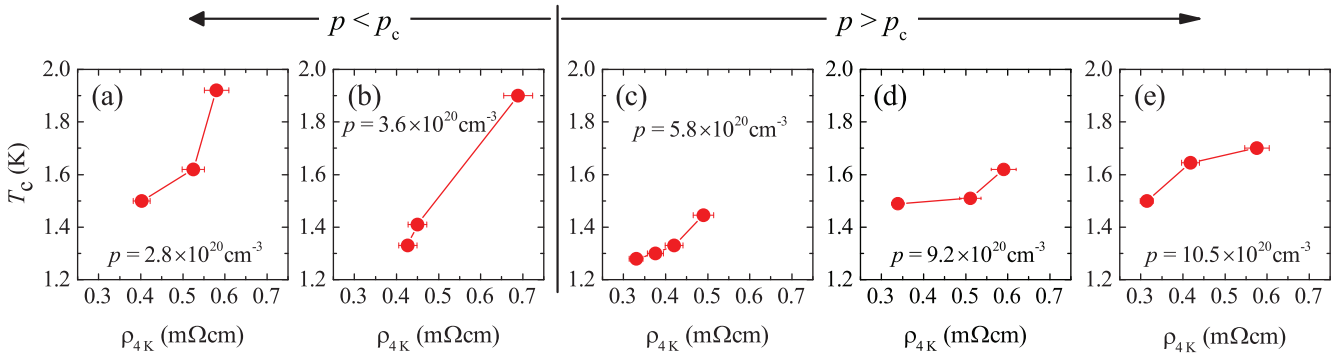

FIG. 3. (Color online) Dependencies of T_c on $\rho_{4\,\mathrm{K}}$ for five p values (in units of 10^{20} cm^{-3}), 2.8, 3.6, 5.8, 9.2, and 10.5. The first two are in the ferroelectric rhombohedral phase ($p < p_c$), while the last three are in the cubic phase ($p > p_c$).

Given that the behavior of T_c for $p < p_c$ is very unusual and that it was previously suggested[26] that bulk superconductivity may not be established in this regime, it is useful to investigate the specific-heat anomaly associated with the superconductivity in this phase. Figure 4(a) shows the temperature dependence of the resistivity ρ_{xx} of a sample in the ferroelectric rhombohedral phase having $p = 3.2 \times 10^{20}$ cm^{-3} ($x = 0.025$), which showed $\rho_{4\,\mathrm{K}} = 0.46$ mΩ cm and $T_c = 1.42$ K with a narrow transition width of 22 mK. The characteristic kink in the $\rho_{xx}(T)$ behavior associated with the structural phase transition[26] is not clearly seen in this sample, probably because the resistivity at the transition is already dominated by impurity scattering rather than by phonon scattering. The specific-heat data of the same sample is shown in Fig. 4(b) in terms of c_{el}/T vs T. Here, c_{el} is the electronic specific heat obtained after subtracting the phonon contribution from the total specific heat.[48] The normal-state electronic specific-heat coefficient $\gamma_{\mathrm{n}} = 0.87$ mJ/mol K^2 is indicated by the dashed line. One notices that c_{el}/T in 0 T approaches zero at low temperature, which gives evidence that this sample is 100% superconducting and that a fully gapped superconductivity can be robustly established even in the ferroelectric rhombohedral phase.

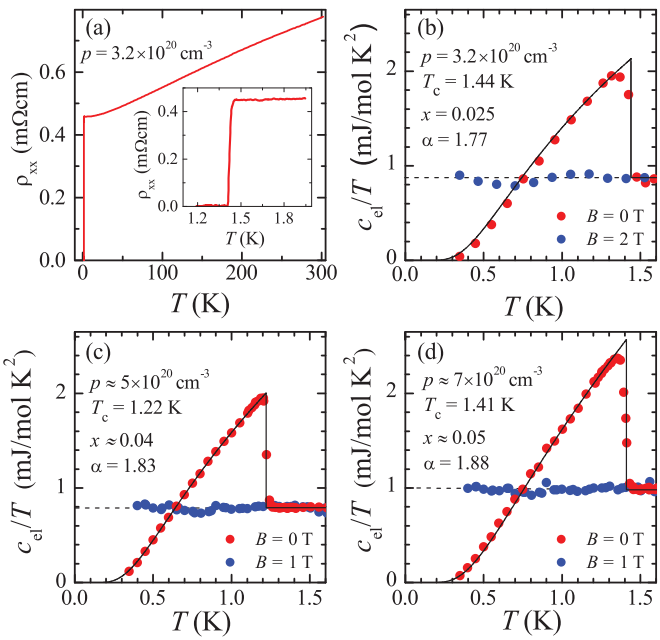

FIG. 4. (Color online) (a) $\rho_{xx}(T)$ of a sample in the ferroelectric rhombohedral phase ($p < p_c$), $p = 3.2 \times 10^{20}$ cm^{-3} ($x = 0.025$); the inset show the sharp superconducting transition at $T_c = 1.42$ K. (b) c_{el}/T vs T of the same sample measured down to 0.34 K in 0 T (red circles) and in 2 T (blue circles). (c), (d) c_{el}/T vs T plots for samples in the cubic phase ($p > p_c$), $p \simeq 5 \times 10^{20}$ cm^{-3} ($x \simeq 0.04$, $T_c = 1.22$ K) and $p \simeq 7 \times 10^{20}$ cm^{-3} ($x \simeq 0.05$, $T_c = 1.41$ K); those samples were only characterized with specific heat. In (b)–(d), solid lines show the modified BCS fits to the experimental data with tunable α, and dashed lines indicate the values of γ_{n}.

The c_{el}/T data in 0 T was fitted with the modified BCS theory[49] which allows variation of the coupling constant α ($\equiv \Delta_0/T_c$, with Δ_0 the superconducting gap at 0 K). The fitting shown in Fig. 4(b) is made so that it correctly reproduces the jump near T_c;[50] the resulting α, 1.77, is essentially the same as the weak-coupling value of 1.76. The data at lower temperature deviate only slightly from the fitting curve, suggesting that the BCS theory gives a reasonably good description of the specific-heat behavior.

To complement the above specific-heat data for the rhombohedral phase, similar data measured on samples in the cubic phase ($p > p_c$) are shown in Figs. 4(c) and 4(d) for $p \simeq 5 \times 10^{20}$ cm^{-3} ($x \simeq 0.04$, $T_c = 1.22$ K) and $p \simeq 7 \times 10^{20}$ cm^{-3} ($x \simeq 0.05$, $T_c = 1.41$ K), respectively. The fittings using the modified BCS theory are again made so that they correctly reproduce the jump near T_c; the obtained α values, 1.83 and 1.88, are larger than that for $x = 0.025$, but otherwise the data are reasonably well described by the modified BCS theory.

Now we discuss the implications of our data. Between the ferroelectric rhombohedral phase and the cubic phase, the difference in the doping dependence of T_c seems to suggest that the pairing mechanism is somewhat different. Such an inference is corroborated by the fact that the unusual enhancement of T_c with impurity scattering is prominently observed in the rhombohedral phase, while this effect is much weaker in the cubic phase. In this regard, it is useful to note that the Martin-Phillips theory[37] for the enhancement of T_c due to impurity scattering is within the framework of the BCS theory, and therefore the superconductivity in the rhombohedral phase is not necessarily unconventional.[51]

We would like to mention that we have measured one sample with $T_c = 1.9$ K in the rhombohedral phase with the same point-contact technique used in Refs. 8 and 18 and found that the spectra present a two-peak structure that is akin to the conventional Andreev reflection spectra described by the Blonder-Tinkham-Klapwijk theory.[52] On the other hand, we have consistently observed a single zero-bias conductance peak in seven samples so far measured with $T_c \simeq 1.2$ K. We therefore speculate that in $Sn_{1-x}In_xTe$ the even- and odd-parity pairing states may be competing and, since the odd-parity state is expected to be suppressed with nonmagnetic impurities,[41–45] the conventional even-parity state wins in samples with high T_c's where impurity scattering is strong. If this is indeed the case, the odd-parity state is realized only in the lowest T_c samples where the impurity scattering is the weakest.

In the ferroelectric rhombohedral phase, there is no Brillouin-zone folding and the Fermi surface volume is expected to be unchanged from that in the cubic phase. Nevertheless, establishment of the ferroelectric phase is accompanied with generations of ferroelectric domains and charge polarizations, which may have something to do with the present observation. In particular, ferroelectric domain boundaries are expected to be pinned by structural defects in crystals, and hence more disordered samples would contain higher densities of ferroelectric domain boundaries to cause strong electron scattering.

It is prudent to note that all the specific-heat data are reasonably well described by the BCS theory throughout the doping range, which implies that the gap magnitude is always nearly isotropic. However, this does not necessarily contradict the possible realization of odd-parity pairing in low T_c samples suggested by the point-contact spectroscopy made on samples with $T_c \simeq 1.2$ K, because the specific-heat behavior is expected to be essentially the same between the isotropic even-parity pairing and the fully gapped odd-parity pairing.[53] In this context, the coupling constant α to phenomenologically explain the data is found to be slightly *larger* in the $T_c = 1.22$ K sample [Fig. 4(c)] compared to the α in the $T_c = 1.44$ K sample [Fig. 4(b)], which is at odds with the natural expectation that stronger coupling leads to higher T_c; this seems to support the idea that the pairing mechanism is different between the two phases.

In summary, we have elucidated the superconducting phase diagram of $Sn_{1-x}In_xTe$ as a function of In doping for $x < 8\%$ and found that the nature of electron pairing is possibly different between the ferroelectric rhombohedral phase ($x \lesssim 3.8\%$) and the cubic phase ($x \gtrsim 3.8\%$). In particular, in the former phase the T_c was found to be strongly *enhanced* with impurity scattering, while such an effect is weaker in the cubic phase where T_c seems to be primarily governed by carrier density. The unusual role of impurity scattering suggests that conventional even-parity pairing is likely to be realized in higher T_c samples and unconventional superconductivity may only be found in cleaner, lower T_c samples.

We thank T. Ueyama and A. A. Taskin for their help in crystal growths, and L. Fu and P. Phillips for helpful discussions. This work was supported by JSPS (KAKENHI 24740237, 24540320, and 25220708), MEXT (Innovative Area "Topological Quantum Phenomena" KAKENHI), and AFOSR (AOARD 124038). M.N. acknowledges financial support from Croatian Science Foundation (Grant No. O-1025-2012).

*mnovak@sanken.osaka-u.ac.jp

†Present address: RIKEN Center for Emergent Matter Science (CEMS), Wako 351-0198, Japan.

‡y_ando@sanken.osaka-u.ac.jp

[1] L. Fu and E. Berg, Phys. Rev. Lett. **105**, 097001 (2010).

[2] L. Hao and T. K. Lee, Phys. Rev. B **83**, 134516 (2011).

[3] T. H. Hsieh and L. Fu, Phys. Rev. Lett. **108**, 107005 (2012).

[4] A. Yamakage, K. Yada, M. Sato, and Y. Tanaka, Phys. Rev. B **85**, 180509(R) (2012).

[5] K. Michaeli and L. Fu, Phys. Rev. Lett. **109**, 187003 (2012).

[6] Y. S. Hor, A. J. Williams, J. G. Checkelsky, P. Roushan, J. Seo, Q. Xu, H. W. Zandbergen, A. Yazdani, N. P. Ong, and R. J. Cava, Phys. Rev. Lett. **104**, 057001 (2010).

[7] L. A. Wray, S.-Y. Xu, Y. Xia, Y. S. Hor, D. Qian, A. V. Fedorov, H. Lin, A. Bansil, R. J. Cava, and M. Z. Hasan, Nat. Phys. **6**, 855 (2010).

[8] S. Sasaki, M. Kriener, K. Segawa, K. Yada, Y. Tanaka, M. Sato, and Y. Ando, Phys. Rev. Lett. **107**, 217001 (2011).

[9] M. Kriener, K. Segawa, Z. Ren, S. Sasaki, and Y. Ando, Phys. Rev. Lett. **106**, 127004 (2011).

[10] M. Kriener, K. Segawa, Z. Ren, S. Sasaki, S. Wada, S. Kuwabata, and Y. Ando, Phys. Rev. B **84**, 054513 (2011).

[11] M. Kriener, K. Segawa, S. Sasaki, and Y. Ando, Phys. Rev. B **86**, 180505 (2012).

[12] L. A. Wray, S. Xu, Y. Xia, D. Qian, A. V. Fedorov, H. Lin, A. Bansil, L. Fu, Y. S. Hor, R. J. Cava, and M. Z. Hasan, Phys. Rev. B **83**, 224516 (2011).

[13] T. Kirzhner, E. Lahoud, K. B. Chaska, Z. Salman, and A. Kanigel, Phys. Rev. B **86**, 064517 (2012).

[14] X. Chen, C. Huan, Y. S. Hor, C. A. R. Sa de Melo, and Z. Jiang, arXiv:1210.6054.

[15] N. Levy, T. Zhang, J. Ha, F. Sharifi, A. A. Talin, Y. Kuk, and J. A. Stroscio, Phys. Rev. Lett. **110**, 117001 (2013).

[16] T. V. Bay, T. Naka, Y. K. Huang, H. Luigjes, M. S. Golden, and A. de Visser, Phys. Rev. Lett. **108**, 057001 (2012).

[17] K. Kirshenbaum, P. S. Syers, A. P. Hope, N. P. Butch, J. R. Jeffries, S. T. Weir, J. J. Hamlin, M. B. Maple, Y. K. Vohra, and J. Paglione, Phys. Rev. Lett. **111**, 087001 (2013).

[18] S. Sasaki, Z. Ren, A. A. Taskin, K. Segawa, L. Fu, and Y. Ando, Phys. Rev. Lett. **109**, 217004 (2012).

[19] L. Fang, C. C. Stoumpos, Y. Jia, A. Glatz, D. Y. Chung, H. Claus, U. Welp, W. K. Kwok, and M. G. Kanatzidis, arXiv:1307.0260.

[20] T. Sato, Y. Tanaka, K. Nakayama, S. Souma, T. Takahashi, S. Sasaki, Z. Ren, A. A. Taskin, K. Segawa, and Y. Ando, Phys. Rev. Lett. **110**, 206804 (2013).

[21] X.-L. Qi and S.-C. Zhang, Rev. Mod. Phys. **83**, 1057 (2011).

[22] Y. Ando, J. Phys. Soc. Jpn. **82**, 102001 (2013).

[23] A. P. Schnyder, S. Ryu, A. Furusaki, and A. W. W. Ludwig, Phys. Rev. B **78**, 195125 (2008).
[24] F. Wilczek, Nat. Phys. **5**, 614 (2009).
[25] G. S. Bushmarina, I. A. Drabkin, V. V. Kompaniets, R. V. Parfenev, D. V. Shamshur, and M. A. Shakhov, Sov. Phys. Solid State **28**, 612 (1986).
[26] A. S. Erickson, J.-H. Chu, M. F. Toney, T. H. Geballe, and I. R. Fisher, Phys. Rev. B **79**, 024520 (2009).
[27] L. Fu, Phys. Rev. Lett. **106**, 106802 (2011).
[28] T. H. Hsieh, H. Lin, J. Liu, W. Duan, A. Bansil, and L. Fu, Nat. Commun. **3**, 982 (2012).
[29] Y. Tanaka, Z. Ren, T. Sato, K. Nakayama, S. Souma, T. Takahashi, K. Segawa, and Y. Ando, Nat. Phys. **8**, 800 (2012).
[30] S. Kashiwaya and Y. Tanaka, Rep. Prog. Phys. **63**, 1641 (2000).
[31] R. Dornhaus, G. Nimtz, and B. Schlicht, *Narrow-Gap Semiconductors*, Springer Tracts in Modern Physics (Springer, New York, 1983), Vol. 98.
[32] K. L. I. Kobayashi, Y. Kato, Y. Katayama, and K. F. Komatsubara, Phys. Rev. Lett. **37**, 772 (1976).
[33] L. Muldawer, J. Nonmet. **1**, 177 (1973).
[34] L. J. Brillson, E. Burstein, and L. Muldawer, Phys. Rev. B **9**, 1547 (1974).
[35] P. B. Allen and M. L. Cohen, Phys. Rev. **177**, 704 (1969).
[36] A. L. Shelankov, Solid State Commun. **62**, 327 (1987).
[37] I. Martin and P. Phillips, Phys. Rev. B **56**, 14650 (1997).
[38] B. B. Houston, R. S. Allgaier, J. Babiskin, and P. G. Siebenmann, Bull. Am. Phys. Soc. **9**, 60 (1964).
[39] For those samples in which the Hall coefficient was not measured, the p value was assigned based on the x value determined from ICP-AES.
[40] In Ref. 26, the highest value of x where the ferroelectric phase was observed was 0.034, which suggests the critical doping x_c^{FE} should be around 0.04.
[41] R. Balian and N. R. Werthamer, Phys. Rev. **131**, 1553 (1963).
[42] A. I. Larkin, JETP Lett. **2**, 130 (1965).
[43] A. P. Mackenzie, R. K. W. Haselwimmer, A. W. Tyler, G. G. Lonzarich, Y. Mori, S. Nishizaki, and Y. Maeno, Phys. Rev. Lett. **80**, 161 (1998).
[44] A. P. Mackenzie and Y. Maeno, Rev. Mod. Phys. **75**, 657 (2003).
[45] Y. Maeno, S. Kittaka, T. Nomura, S. Yonezawa, and K. Ishida, J. Phys. Soc. Jpn. **81**, 011009 (2012).
[46] P. W. Anderson, J. Phys. Chem. Solids **11**, 26 (1959).
[47] C. M. Varma, Phys. Rev. Lett. **61**, 2713 (1988).
[48] The total specific heat c_p in the normal state after suppressing the superconductivity in 1 or 2 T was fitted with the Debye formula $c_p = \gamma_{\mathrm{n}} T + A_3 T^3 + A_5 T^5$, where A_3 and A_5 are the coefficients of the phononic contribution. The fitting parameters for the samples shown in Figs. 4(b)–4(d) are $[\gamma_{\mathrm{n}}(\mathrm{mJ/mol\,K^2}), A_3(\mathrm{mJ/mol\,K^4}), A_5(\mathrm{mJ/mol\,K^6})] = (0.874, 0.655, 0.016)$, (0.786, 0.704, 0.007), and (0.982, 0.578, 0.014), respectively.
[49] H. Padamsee, J. E. Neighbor, and C. A. Shiffman, J. Low Temp. Phys. **12**, 387 (1973).
[50] From the data in Figs. 4(a) and 4(b), we can estimate the effective mass via $m^* = (3\hbar^2\gamma_{\mathrm{n}})/(V_{\mathrm{mol}} k_B^2 k_F) = 3.4 m_e$ ($V_{\mathrm{mol}} = 38\ \mathrm{cm^3/mol}$ is the molar volume and m_e is the free electron mass) by approximating the Fermi wave number $k_F = [3\pi^2(p/4)]^{1/3} = 1.3\ \mathrm{nm^{-1}}$, for which spherical Fermi surfaces located at the four L points are assumed. The mean free path $\ell = \hbar k_F/(\rho_{4\,\mathrm{K}} p e^2) = 3.9$ nm is much shorter than the coherence length $\xi_0 = \hbar v_F/(\pi\alpha k_B T_c) = 38$ nm.
[51] The γ_{n} value for $x = 0.025$ [Fig. 4(b)] is larger than that for $x \simeq 0.04$ [Fig. 4(c)] despite the lower carrier density, which is consistent with the notion (Ref. 37) that an enhancement of the density of states is responsible for higher T_c.
[52] G. E. Blonder, M. Tinkham, and T. M. Klapwijk, Phys. Rev. B **25**, 4515 (1982).
[53] T. Hashimoto, K. Yada, A. Yamakage, M. Sato, and Y. Tanaka, J. Phys. Soc. Jpn. **82**, 044704 (2013).